Neurobiology of Disease 132 (2019) 104542

Contents lists available at ScienceDirect

Neurobiology of Disease

journal homepage: www.elsevier.com/locate/ynbdi

Periodic dietary restriction ameliorates amyloid pathology and cognitive impairment in PDAPP-J20 mice: Potential implication of glial autophagy

Amal Gregosa[a,b,c], Ángeles Vinuesa[a,b], María Florencia Todero[d], Carlos Pomilio[a,b], Soledad P. Rossi[a,e], Melisa Bentivegna[a,b], Jessica Presa[a,b], Shirley Wenker[f], Flavia Saravia[a,b], Juan Beauquis[a,b,*]

[a] Instituto de Biología y Medicina Experimental, CONICET, Buenos Aires, Argentina
[b] Departamento de Química Biológica, Facultad de Ciencias Exactas y Naturales, Universidad de Buenos Aires, Argentina
[c] Cátedra de Anatomía e Histología, Facultad de Farmacia y Bioquímica, Universidad de Buenos Aires, Argentina
[d] Laboratorio de Fisiología de los Procesos Inflamatorios, Instituto de Medicina Experimental (IMEX), CONICET, Academia Nacional de Medicina, Buenos Aires, Argentina
[e] Cátedra de Bioquímica Humana, Facultad de Medicina, Universidad de Buenos Aires, Argentina
[f] Fundación Instituto Leloir-IIBA, CONICET, Buenos Aires, Argentina

ARTICLE INFO

Keywords:
Alzheimer's disease
Nutrient restriction
Memory
Amyloid
Astroglia
Autophagy

ABSTRACT

Dietary restriction promotes cell regeneration and stress resistance in multiple models of human diseases. One of the conditions that could potentially benefit from this strategy is Alzheimer's disease, a chronic, progressive and prevalent neurodegenerative disease. Although there are no effective pharmacological treatments for this pathology, lifestyle interventions could play therapeutic roles. Our objectives were 1) to evaluate the effects of dietary restriction on cognition, hippocampal amyloid deposition, adult neurogenesis and glial reactivity and autophagy in a mouse model of familial Alzheimer's disease, and 2) to analyze the role of glial cells mediating the effects of nutrient restriction in an *in vitro* model. Therefore, we established a periodic dietary restriction protocol in adult female PDAPP-J20 transgenic mice for 6 weeks. We found that dietary restriction, not involving overall caloric restriction, attenuated cognitive deficits, amyloid pathology and microglial reactivity in transgenic mice when compared with *ad libitum*-fed transgenic animals. Also, transgenic mice showed an increase in the astroglial positive signal for LC3, an autophagy-associated protein. In parallel, hippocampal adult neurogenesis was decreased in transgenic mice whereas dietary-restricted transgenic mice showed a neurogenic status similar to controls. *In vitro* experiments showed that nutrient restriction decreased astroglial and, indirectly, microglial NFκB activation in response to amyloid β peptides. Furthermore, nutrient restriction was able to preserve astroglial autophagic flux and to decrease intracellular amyloid after exposure to amyloid β peptides. Our results suggest neuroprotective effects of nutrient restriction in Alzheimer's disease, with modulation of glial activation and autophagy being potentially involved pathways.

1. Introduction

Alzheimer's disease (AD) is a chronic, progressive pathology characterized by brain protein aggregation associated to neurodegenerative changes, ultimately leading to cognitive impairment and dementia. Its main histopathological hallmarks are cerebral amyloid deposition and intraneuronal neurofibrillary tangles. Early in the progression of the disease, astrocytes and microglia lose their homeostatic and neuroprotective functions and promote inflammation, even before amyloid β (Aβ) deposition (Beauquis et al., 2014; Olabarria et al., 2010; Pomilio et al., 2016). At later stages, extensive neurodegeneration leads to dementia.

Although there are no effective treatments for AD, lifestyle changes were described in association with reductions in its incidence and progression. Among these, routinely carrying out physical, social and intellectual activities is one of the most promising strategies to delay disease progression (Ngandu et al., 2015). In recent years, attention has been put into dietary restriction (DR) as a potential neuroprotective

Abbreviations: Aβ, Amyloid beta; AD, Alzheimer's disease; AL, *Ad libitum* diet; APP, Amyloid precursor protein; BAF, Bafilomycin A1; CM, Conditioned medium; CTL, Control; DCX, Doublecortin; DG, dentate gyrus; DR, Dietary restriction; GCL, Granular cell layer; GFAP, Glial fibrillary acidic protein; NR, Nutrient restriction; NTg, Non-transgenic; SGZ, Subgranular zone; Tg, Transgenic

* Corresponding author at: Instituto de Biología y Medicina Experimental, Vuelta de Obligado 2490, 1428 Buenos Aires, Argentina.
E-mail addresses: juanbeauquis@gmail.com, beauquis@dna.uba.ar (J. Beauquis).

https://doi.org/10.1016/j.nbd.2019.104542
Received 25 March 2019; Received in revised form 30 June 2019; Accepted 22 July 2019
Available online 24 July 2019

strategy. Evidence suggests that DR of food intake could lead to the prevention of chronic diseases and to increase longevity in different animal models (Mattson, 2005; McCay et al., 1935), modulating energy metabolism, antioxidant defenses, inflammation and autophagy, among other pathways (Liu et al., 2017). Moreover, DR can prevent age-related alterations in motor and cognitive function, dendritic plasticity and glial function in rats and mice (Ma et al., 2018; Mladenovic Djordjevic et al., 2010; Moroi-Fetters et al., 1989), potentially reducing the impact of age-associated diseases. Results from human studies and animal models suggest that DR could prevent AD-associated brain changes through multiple mechanisms including neuroprotection, glial modulation and amyloid clearance (Halagappa et al., 2007; Luchsinger et al., 2002; Patel et al., 2005). One of the processes that results upregulated after DR is autophagy, a catabolic mechanism that degrades and recycles organelles and misfolded proteins like Aβ and could play a role in its clearance from tissues (Nilsson et al., 2013). Interestingly, AD-associated phenomena like inflammation and glial activation can have an effect on autophagy functionality, further amplifying neurodegeneration (Alirezaei et al., 2011).

Despite the plethora of health benefits that have been described in association to caloric restriction, one important concern is the effect of this strategy on body weight and energy metabolism. As in other age-associated diseases, weight loss could be a relevant issue in the context of AD, eventually increasing the burden of the disease (Tamura et al., 2007). Most DR protocols involve caloric restriction and consequently lead to weight loss in variable percentages. Therefore, periodic schedules of DR that do not induce an overall decrease of caloric intake are potentially clinically-translatable alternatives (Brandhorst et al., 2015).

In the present work our objective was to study the effects of a periodic DR protocol, which does not induce weight loss, on the modulation of experimental AD-associated cognitive and brain changes in a transgenic mouse model of the pathology. Complementarily, an *in vitro* approach was implemented to analyze glial responses to amyloid exposure and nutrient restriction. We studied astroglial autophagy and Aβ content in autophagosomes as evidences of a potential clearance pathway, and microglial activation as a pathogenic and modifiable event in experimental AD.

2. Materials and methods

2.1. Animals

Female adult PDAPP-J20 (PDGFB-APPSwInd) transgenic (Tg) mice and their non-transgenic (NTg) siblings were obtained from our colony at the animal facility of the Institute of Biology and Experimental Medicine (IBYME-CONICET; NIH Assurance Certificate # A5072-01). Breeders were provided by Dr. Verónica Galván from the University of Texas San Antonio Health Science Center. These mice carry the amyloid precursor protein (APP) human gene with Swedish and Indiana mutations for familial AD obtained through crossing hemizygous transgenic males with C57BL/6 J (Jackson Lab.) female mice (Mucke et al., 2000). Transgenic mice were genotyped through PCR with specific human APP primers. Non-transgenic mice were used as controls. Animals were housed in groups of 3 to 5 individuals per cage with controlled humidity and temperature under a standard light/dark cycle with lights on at 7 a.m. All animal experiments followed the NIH Guide for the Care and Use of Laboratory Animals (https://www.ncbi.nlm.nih.gov/books/NBK54050) and were approved by the Ethical Committee of the Institute of Biology and Experimental Medicine. Every effort was made to reduce the number of mice used in the study as well as to minimize animal suffering and discomfort.

2.1.1. Experimental protocol

Female 6.5 month-old Tg and NTg mice were divided into *ad libitum* (AL) or dietary restriction (DR) groups. All animals were fed standard rodent chow (GEPSA Feeds, Pilar, Argentina) from weaning until the end of the experimental protocol at 8 months of age. Daily food intake was measured during the last 5 days before starting the restriction protocol in order to calculate the 60% intake amount that was later provided during the DR periods. The periodic DR protocol is depicted in Fig. 1 A. Individuals in the DR group underwent 3 cycles of DR-AL periods with each cycle lasting 2 weeks and consisting of 5 days of DR followed by 9 days of AL diet. The areas under the curve for food intake in each period were calculated using Prism 7.0 (GraphPad Software Inc.). *Ad libitum*-fed mice had free access to food pellets during all the experimental protocol. Weight and fasting glycemia were measured before the beginning of the DR protocol and before euthanasia using a glycometer (One Touch Ultra, Johnson & Johnson, Argentina). Euthanasia was performed at the end of the experimental protocol by injection of ketamine (80 mg/kg BW, i.p.; Holliday-Scott, Argentina) and xylazine (10 mg/kg BW, i.p.; Bayer, Argentina) and transcardial perfusion with 0.9% NaCl followed by 4% paraformaldehyde.

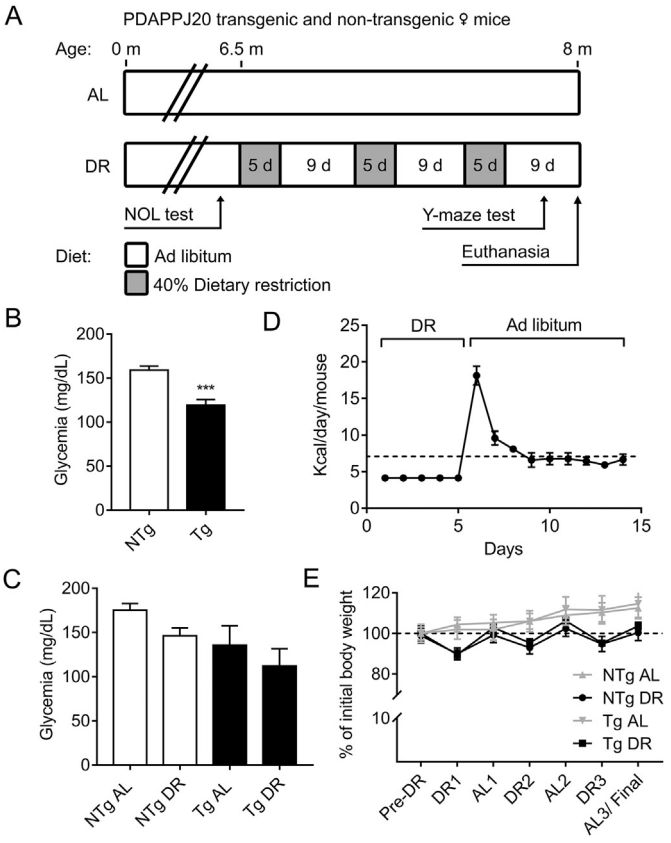

Fig. 1. A. Experimental design. AL: *ad libitum*; DR: dietary restriction; NOL: Novel object-location recognition test. Fasting Glycemia before DR at 6.5 months of age. ***$p < .001$ (Student's *t*-test). C. Fasting glycemia at 8 months of age. D. Mean daily food intake (Kcal) per mouse during DR and AL periods. The dotted line represents 6.875 Kcal corresponding to mean daily food intake per mouse measured for one week before starting the DR protocol. E. Body weight percent change before DR (pre-DR), at the end of each DR period (DR1, DR2 and DR3) and at the end of each AL period (AL1, AL2 and AL3/final weight), $n = 5–11$ animals per group.

2.1.2. Behavioral evaluation

Behavioral testing was done at 5 and 8 months of age in order to evaluate the cognitive status before and after the dietary intervention ($n = 8$ per group). At 5 months of age we conducted a novel object-location recognition test (NOL) in groups of Tg and NTg mice as previously published (Beauquis et al., 2014). Mice were tested in a black plastic box ($30 \times 30 \times 30\ cm^3$) to which they were adequately habituated for 6 days prior to the trial. The test consisted of two 10-min trials (sample trial or T1 and test trial or T2) separated by a 1-h inter-

trial interval (short-term memory). In T1, mice were exposed to two identical plastic objects that were placed in two selected contiguous corners, whereas during T2, one of the objects was moved to a novel location in the opposite corner respective to the non-displaced object. Exploration of the objects was considered positive when the animals' snout was facing the objects at < 1 cm away. Performance was assessed as the percentage of time exploring the object in the novel location to total exploration time in T2. Exploration of the objects in T1 was quantified in order to determine the correct habituation to the objects, establishing 20 s as the inclusion time criteria. Also non-preference for any of the objects/box sectors in T1 was confirmed. In the last week of the protocol at 8 months of age and when all the groups were fed *ad libitum*, behavioral testing was done using the Y-maze task (Vinuesa et al., 2016). We did not run the NOL test at this time point in order to avoid a possible interference of the past experience of these mice in the test arena. The Y-maze apparatus consisted of a black maze with three 30 cm long-arms in an equal angled disposition. Mice were adequately habituated to the room where the tests are carried out. The test consisted of two 10-min trials (sample trial or T1 and test trial or T2), separated by a 4-h inter-trial interval (intermediate-term memory). During T1, mice were allowed to explore two of the three arms, while during T2, exploration of the third novel arm was permitted. Having verified that exploration in T1 was not different from the 50% in either arm, behavior in T2 was evaluated as the percentage of time exploring the novel arm to total exploration time in T2. Locomotor activity, measured as total distance, was assessed in both tests with Any-maze video tracking system (Stoelting Co., USA) and no differences were found between groups.

2.1.3. Tissue processing, Congo red staining and immunohistochemistry

After euthanasia, brains were dissected out of the skull and the hemispheres were separated. Hippocampi were dissected from the left hemispheres and frozen in dry ice for protein analysis. The right hemispheres were fixed overnight with paraformaldehyde 4%, coronally cut at 60 μm using a vibrating microtome (PELCO easiSlicer, Ted Pella, USA) and sections corresponding to the hippocampus were stored in cryoprotectant solution (PBS:ethylene glycol:glycerine 2:1:1), at −20 °C until use for histological analyses. Congo red staining was done to detect brain amyloid deposition as previously published (Pomilio et al., 2016). Immunohistochemistry and immunofluorescence were performed on 6 serial brain sections per mouse using a free-floating technique for doublecortin (goat polyclonal, 1:500, sc-8066, SCBT, USA), GFAP (rabbit polyclonal, 1:300, G-9269 or mouse monoclonal, 1:300, G-3893, Sigma, USA), Iba1 (rabbit polyclonal, 1:1500, Wako Chemicals, Japan), LC3 (rabbit polyclonal, 1:500; NB100–2331, Novus Biologicals, USA) and Aβ (4G8 mouse monoclonal, 1:1000, MAB1561, Chemicon, USA). Briefly, sections were thoroughly rinsed in PBS to eliminate cryoprotectant solution before blocking of unspecific antigenic sites with rabbit (for DCX) or goat (for GFAP and Iba1) normal serum. For DCX staining, inhibition of endogenous peroxidase was done by incubating sections in Metanol:PBS:H_2O_2 (1:1:0.1). Sections were incubated overnight with primary antibodies and subsequently with corresponding secondary biotinylated (anti-goat, anti-rabbit and anti-mouse; 1:1000, Vector Labs, USA) or fluorescent (Alexa 488/555 anti-rabbit and anti-mouse, 1:1000, Invitrogen, USA) antibodies.

2.1.4. Histological analyses

2.1.4.1. Quantification of hippocampal amyloid load. Microphotographs of the hippocampus were obtained from Congo red stained serial brain sections using a Nikon E-200 microscope. For amyloid load estimation, the total area of the dentate gyrus and its Congo red-positive subarea were measured on spatially calibrated images with a user-defined threshold to identify stained areas using ImageJ software (Abramoff et al., 2004). The results were expressed as the percentage of the dentate gyrus area covered by Congo red + amyloid deposits ($n = 5$ per group). The total number of Congo red + deposits was estimated using Cavalieri's principles on serial hippocampus sections and also the size-distribution of plaques was calculated.

2.1.4.2. Doublecortin + cell counting. Doublecortin-positive cells were counted in the subgranular zone (SGZ) and granular cell layer (GCL) of the dentate gyrus (DG) under a 40× objective using a Nikon E-200 microscope. Every eighth 60 μm coronal brain section throughout the entire rostrocaudal extension of the DG were analyzed in each mouse ($n = 5$ per group). The total number of cells was estimated using Cavalieri's principle. Both upper and lower blades of the GCL and SGZ were considered for cell counting. The results are shown for dorsal and ventral dentate gyrus separately and expressed as the total number of DCX + cells in each compartment.

2.1.4.3. GFAP immunoreactive area and Sholl analysis. Immunoreactive area of GFAP + astrocytes was calculated using a user-defined threshold on 8-bit bright-field images of hippocampal sections ($n = 5$ per group). Results were expressed as the percentage of the hilus region covered by GFAP + areas. Sholl analysis of GFAP + cells was done following previously published protocols (Beauquis et al., 2010). Briefly, multiple confocal planes were obtained from GFAP-fluorescently stained hippocampal sections and averaged to generate *Z*-stacks. Averaged images were traced to obtain binary versions devoid of background staining, scaled and analyzed with ImageJ running Sholl Analysis Plugin (written by Tom Maddock; Ferreira et al., 2014). A minimum of 25 GFAP + cells per animal were evaluated (n = 5 per group). Results were expressed as the mean number of intersections per each radius-defined circle.

2.1.4.4. LC3 content in hippocampal astrocytes. Quantification of hippocampal LC3 and GFAP astroglial levels was done on confocal images of GFAP-LC3 immunofluorescence (n = 5 per group). Manders' coefficient was calculated using the JACoP plug-in (Bolte and Cordelieres, 2006) for ImageJ software on thresholded images. Results were expressed as the M2 coefficient representing the proportion of the GFAP + area that was also positive for LC3.

2.1.4.5. Iba1 + microglial density and morphology. Microglial soma size was measured on calibrated microphotographs from randomly chosen individual cells in the hilus of the DG. Somata were delineated and their surface quantified using ImageJ software. Activation score was calculated using a previously published protocol (Pomilio et al., 2016). Briefly, three microglial morphological activation phenotypes were defined: ramified (non-activated), reactive, and ameboid, representing progressive activation stages (Fig. 4 D). Using a randomly placed $6 \times 10^5\ \mu m^3$ counting probe, the proportion of each phenotype was analyzed. The activation score was calculated as the sum of the multiplication of each morphology proportion by a numerical factor: 0 for ramified, 1 for reactive and 2 for ameboid. At least 50 cells were measured in each animal ($n = 5$ per group).

2.1.5. Immunoblotting

Interleukin 1 β (IL1β) contents were determined in hippocampi by immunoblotting. Samples were homogenized by sonication in supplemented RIPA buffer and protein levels were quantified using the Bradford method (Bradford, 1976). Then, after lysis with loading buffer, homogenates were loaded onto 12% acrylamide gels, separated by SDS-PAGE and transferred to nitrocellulose membranes. Membranes were blocked with 5% non-fat milk in TBS 0.5% Tween-20 and then incubated overnight at 4 °C with antibodies raised against IL1β (mouse monoclonal, 1:500 sc-32,294, SCBT) or β-Actin (mouse monoclonal, 1:500, sc-47,778, SCBT). After rinsing, membranes were incubated with an HRP-conjugated secondary antibody (goat anti mouse, 1:2000, sc-2064, SCBT) for 1 h. Immunoreactivity was visualized with detection reagents (luminol and p-coumaric acid; Sigma, USA) using an Amersham Imager 600 RGB (GE Healthcare, USA). Bands were quantified

using the ImageJ plugin for gel analysis and ratios of IL1β/β-actin (n = 5 hippocampi per group) levels were calculated.

2.2. Cell culture

Astroglial and microglial *in vitro* experiments were done using C6 and BV2 cell lines, respectively. Rat astrocytoma C6 cell line (ATCC CCL-107) (Benda et al., 1968) was kindly provided by Dr. Zvi Vogel (Weizmann Institute of Science, Israel) to Dr. Kotler. Mouse BV2 microglial cell line was provided by Dr. Guillermo Giambartolomei (Hospital de Clínicas, Buenos Aires, Argentina). Both cell lines were cultured in RPMI 1640 medium (Gibco, USA) supplemented with 10% Fetal Bovine Serum (FBS; Internegocios SA, Argentina), 2.0 mM glutamine, 100 units/mL penicillin and 100 mg/mL streptomycin. Cells were cultured at 37 °C in a humidified atmosphere of 5% CO_2/95% air.

2.2.1. Nutrient restriction, amyloid β exposure and bafilomycin treatment

Nutrient restriction (NR) was performed by incubation of astrocytes or microglia with RPMI + 2% FBS (control medium: RPMI + 10% FBS) for 6 h. Afterwards, cells were exposed to Aβ 1–42 peptides (A9810, Sigma, USA), pre-fibrilized by incubation in water at 37 °C for 72 h, using two different protocols. For the collection of astrocyte-derived conditioned medium (CM), amyloid peptides were adsorbed to nitrocellulose at the bottom of the plate to ensure an amyloid-free medium to subsequently stimulate microglia (Combs et al., 2001). Briefly, 1 cm^2 of nitrocellulose (GE, USA) was dissolved in methanol, pipetted to the bottom of culture wells and allowed to dry before adding Aβ peptides at 3 μM (Lagenaur and Lemmon, 1987). After rinsing, cells were seeded and exposed to the peptide for 24 h. Conditioned medium was collected, centrifuged and used at a 1:1 dilution in complete RPMI medium to stimulate BV2 microglia for 2 (NFκB immunocytochemistry) or 24 h (MTT assay). For NFκB immunocytochemistry on astrocytes, Aβ peptides were dissolved in the culture medium at 0.5 μM for a 2 h-exposure after NR (or non-restricted conditions). Fixation was achieved by incubation with ice-cold methanol for 5 min. For studying astroglial autophagy, NR was done for 6 h on C6 cells, as detailed previously, prior to Aβ 1–42 or control medium incubation for 2, 6 or 24 h to understand the progression of the process. A group of NR Aβ cells in each protocol were treated with bafilomycin A1 (BAF; Fermentek, Israel), a negative regulator of the autophagic flux that inhibits lysosomal degradation, to determine if the effects of NR required a functional autophagy. Treatment with BAF was done at a 100 nM dose for the last 2 h of Aβ incubation.

2.2.2. MTT viability assay

3-(4,5-Dimethyl-thiazol-2-yl)22,5-diphenyl-tetrazolium bromide (MTT) reduction assay was carried out according to the previously described protocol (Pomilio et al., 2016). After exposure to astrocyte CM, microglial cells were grown on 96-well plates, rinsed with PBS and incubated with MTT (Sigma, USA) 0.125 mg/mL in RPMI media for 90 min at 37 °C. Then, the product formazan was solubilized in DMSO and absorbance was measured at 570 nm with background subtraction at 655 nm in a BIO-RAD Model 680 Benchmark microplate reader (Bio-Rad Laboratories, USA). The MTT reduction activity was expressed as a relative ratio to RPMI-incubated cell absorbance.

2.2.3. Immunocytochemistry

After fixation with methanol, NFκB immunocytochemistry was performed on C6 and BV2 cells to determine nuclear translocation as a proxy for cell activation. Immunofluorescence against Aβ/LC3 was done on C6 cells to determine if intracellular Aβ was associated to autophagic vesicles as previously reported (Pomilio et al., 2016). Cells attached to coverslips were permeabilized with 0.5% triton X-100 in PBS and unspecific binding sites were blocked with 1% BSA in PBS. Cells were incubated with primary antibodies for LC3 (rabbit polyclonal, 1:1000; NB100-2331, Novus Biologicals, USA), Aβ (4G8 mouse monoclonal, 1:1000, MAB1561, Chemicon, USA) or NFκB (rabbit polyclonal, 1:1000, sc-372, SCBT, USA) and then with Alexa Fluor (488/596; Invitrogen, Thermo Fisher, USA) labeled secondary antibodies. Nuclei were visualized with DAPI (D9542, Sigma, USA) and coverslips were mounted on glass slides with PVA-DABCO (Sigma, USA).

2.2.4. Quantification of immunoflorescence images

Quantification of LC3-Aβ immunofluorescence was done using ImageJ software. Individual cell areas from spatially calibrated images were outlined and measured before applying a threshold to measure immunopositive areas for each fluorophore. The analysis of co-localization between both markers was done using JACoP plug-in and expressed as the percentage or Aβ + areas that were also positive for LC3 (M2 Mander's coefficient). Nuclear translocation of NFκB was evaluated by measuring the optical density on 8-bit grayscale images (OD; 0 = black, no staining; 255 white, max. staining) of the specific NFκB staining on the nucleus and on the cytoplasm of each cell. Then, results were expressed as the nucleus OD/cytoplasm OD ratio. Higher values indicated higher nuclear translocation.

2.3. Statistical analysis

The acquisition and analysis of experimental data were performed under blind conditions regarding group information. Statistical analyses involved unpaired one-tailed Student's *t*-test, two-way ANOVA with Tukey's or Dunnett's *post hoc* tests or repeated measures (RM)- ANOVA, as detailed for each experiment in the Results section, and were performed with Prism 7.0 (GraphPad Software Inc.). Data are expressed as mean ± SEM. The sample size was calculated using StatMate 2.0 (GraphPad Software Inc.) considering the results from our previous studies to obtain a 5% statistical significance with 80% statistical power to detect differences of at least 10% between groups. Group size is detailed in figure legends for each experiment.

3. Results

3.1. Glycemia and body weight are not significantly affected by dietary restriction

Glycemia at 6.5 months of age, before commencing the DR, was lower in Tg compared with NTg mice (Student's *t*-test, $p < .01$; Fig. 1 B). Comparison of glucose levels at the end of the last AL period showed a genotype effect (Two-way ANOVA, $p < .01$; Fig. 1 C) without differences within genotypes (Tukey's *post hoc* test). Food intake for the DR groups was measured during each AL period after DR to check for a compensation effect. A rebound effect was noticed predominantly on the first and second days of the AL period with a normalization of food intake from the third day onwards (Fig. 1 D). Mean Kcal consumed per mouse daily during DR-AL cycles was compared with pre-DR daily intake and no differences were found (One-sample Student's *t*-test, DR + AL cycle 6.87 *vs.* pre-DR 6.82 Kcal/day/mouse, $p = .75$) indicating the absence of overall caloric restriction with this diet. Moreover, areas under curve for DR and AL periods were similar (DR −13.2 ± 1.97 *vs.* AL 13.94 ± 1.87, net area 0.74, CI 95% = 0–6.057). Body weight was measured at the beginning and at the end of each DR/AL period. Although a slight ~10% decrease in body weight was evident at the end of each DR period and a compensatory increase after each AL period, mice did not show weight loss at the end of the experimental protocol (RM-ANOVA for weight evolution and Tukey's *post hoc* test for the comparison of the percentage change in final/initial body weight, $p = .98$ for NTg and $p = .89$ for Tg under DR; Fig. 1 E). Mice under the *ad libitum* diet showed a 10–15% increase in body weight at the end of the protocol when compared with their initial weight (Tukey's *post hoc* test, $p < .0001$ both for NTg and Tg under AL diet).

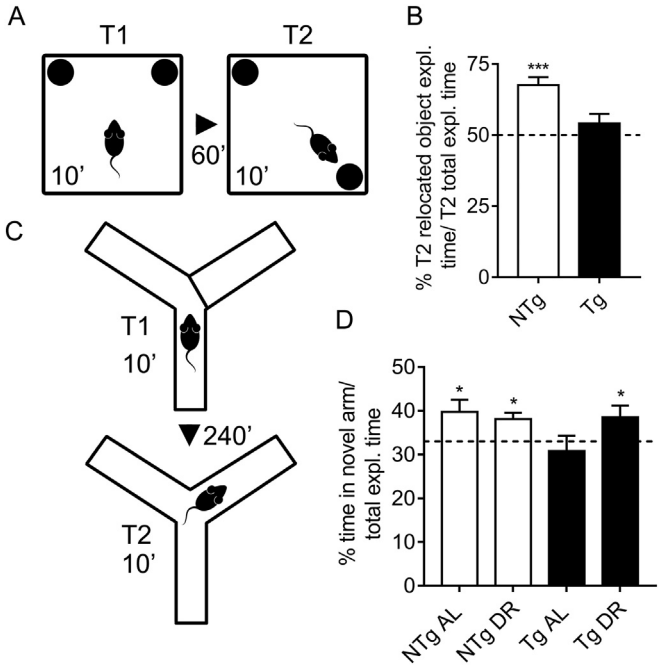

Fig. 2. A. Graphical representation of the novel object-placement recognition test. During the acquisition phase (T1) mice were allowed to explore both objects for 10 min and then returned to their home cages for 60 min. In the test phase (T2) one object was displaced and exploration time was measured for 10 min. B. Performance expressed as the percentage of the relocated object exploration time/total exploration time. ***p < .001 *vs.* 50% theoretical mean as the chance level (one-sample Student's t-test). C. Graphical representation of the Y-maze test. During the acquisition phase (T1) mice were allowed to explore two arms of the arena for 10 min and then returned to their home cages for 240 min. In the test phase (T2), access to the previously blocked arm was allowed and exploration time was measured for 10 min. D. Performance expressed as the percentage of novel arm exploration time/total exploration time *$p < .05$ *vs.* 33% theoretical mean as the chance level (one-sample Student's *t*-test), $n = 7–10$ animals per group.

3.2. Dietary restriction ameliorates memory deficits of transgenic mice

At 5 months of age, 6 weeks before the beginning of the dietary intervention, mice were tested with the novel object-placement recognition task to analyze hippocampus-dependent spatial memory. Control mice showed a significant preference for the displaced object ($p < .001$, one-sample Student's *t*-test *vs.* 50% theoretical mean; Fig. 2 A-B) while transgenic mice performed at chance level ($p > .05$), indicating an impairment of spatial memory. At 8 months of age, after finishing the diet protocol, spatial memory was evaluated using a Y-maze test analyzing the exploration time of the novel arm. Non-transgenic mice both under AL and DR regimens preferentially explored the novel arm of the maze ($p < .05$ *vs.* 33% chance level; Fig. 2 C-D). Exploration time of the previously blocked arm by *ad libitum*-fed transgenic mice was at chance level (p > .05, one-sample Student's *t*-test *vs.* 33% chance level) suggesting an inability to recognize it as a novel environment. However, dietary restricted transgenic mice were able to identify the novel arm, evidenced by an increased preference (p < .05 *vs.* 33% chance level).

3.3. Dietary restriction prevents the impairment of adult neurogenesis in APP transgenic mice

In order to study the potential implication of adult hippocampal neurogenesis as a subjacent process for the cognitive changes described in the previous section, we performed an immunohistochemistry for doublecortin (DCX) on coronal brain sections (Fig. 3 A). The number of

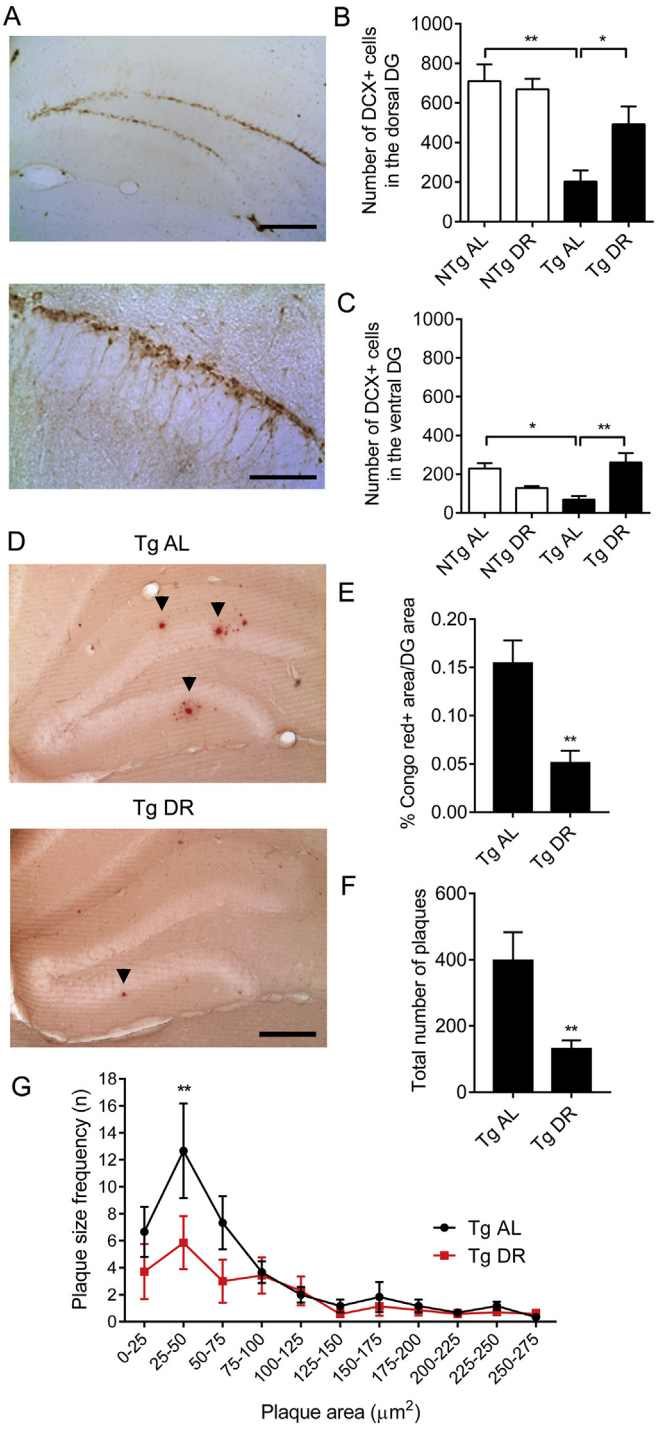

Fig. 3. A. Representative microphotographs of DCX immunostained neurons in the dentate gyrus. Scale bars: 200 μm (upper panel) and 80 μm (lower panel). B and C. Number of DCX+ cells in the dorsal (B) and ventral (C) dentate gyrus. *p < .05; **$p < .01$ (Tukey's *post hoc* test, two-way ANOVA). D. Hippocampus coronal sections showing Congo red staining for amyloid in transgenic mice under *ad libitum* (AL) or restriction (DR) diets. Arrowheads indicate amyloid plaques in the dentate gyrus. Scale bar: 300 μm. E. Amyloid load in the dentate gyrus. F. Number of Congo red+ plaques in the dentate gyrus. **$p < .01$ (Student's *t*-test). G. Size distribution of Congo red+ plaques. **p < .01 at the 25–50 μm^2 size range, Bonferroni's *post hoc* test, RM two-way ANOVA), $n = 5–7$ animals per group. (For interpretation of the references to colour in this figure legend, the reader is referred to the web version of this article.)

DCX+ cells was quantified in the dorsal and ventral dentate gyrus and the analysis showed that Tg AL mice had fewer number of cells compared with NTg AL animals in both compartments ($p < .01$ for dorsal DG and $p < .05$ for ventral DG, Tukey's *post hoc* test, two-way ANOVA, Fig. 3 B–C). Dietary restriction in transgenic animals led to a DCX cell number similar to control levels and different from Tg AL ($p < .05$ for dorsal DG and $p < .01$ for ventral DG, Tukey's *post hoc* test). A tendency towards a decrease in the number of DCX+ cells in the ventral DG of NTg DR mice was noted although this difference was not statistically significant ($p = .14$ *vs.* NTg AL, Tukey's *post hoc* test).

3.4. Dietary restriction is associated with a decreased amyloid load in the hippocampus

Congo red staining was performed to detect amyloid deposition in the hippocampus of Tg mice (Fig. 3 D). Non-transgenic controls did not show detectable staining. Transgenic mice that underwent dietary restriction showed significantly less number of amyloid deposits as well as a diminished amyloid load (% Congo red area/reference area) in the dentate gyrus of the hippocampus compared with the Tg AL group ($p < .01$ for both comparisons, Student's *t*-test, Fig. 3 E–F). The analysis of the size-distribution of plaques showed that the effect of DR was predominant on the 25–50 μm^2 size range ($p < .01$, Bonferroni's *post hoc* test, RM two-way ANOVA, Fig. 3 G).

3.5. Astroglial morphology in the hippocampus

The analysis of GFAP immunostained astrocytes was done by evaluating the immunoreactive area and the cell processes complexity (Sholl analysis) in the hilus of the hippocampus (Fig. 4 A). Regarding GFAP immunoreactive area, a genotype effect was found (Two way ANOVA, $p < .01$, Fig. 4 B) with both Tg AL and Tg DR groups showing increased levels compared with NTg AL ($p < .05$, Tukey's *post hoc* test). No differences were found between groups in the processes complexity (RM ANOVA, Fig. 4 C).

3.6. Increased microglial soma area in transgenic mice is prevented by dietary restriction

We analyzed microglial soma area in the hilus of the dentate gyrus on Iba1 immunostained brain sections (Fig. 4 D). The analysis of this parameter showed that transgenic animal fed *ad libitum* had larger microglial cells than control mice ($p < .05$ Tg AL *vs.* NTg AL, Tukey's *post hoc* test, two-way ANOVA; Fig. 4 E). Interestingly, microglial soma areas of transgenic mice under dietary restriction were not different from control microglia. We evaluated microglial activation by means of a morphological score (Fig. 4 F) and found a genotype effect (two-way ANOVA, $p < .01$) with no differences between individual groups (Tukey's *post hoc* test).

3.7. Dietary restriction is associated with lower IL1β levels in the hippocampus

We analyzed hippocampal IL1β protein levels by immunoblotting and found that DR groups showed lower levels than AD groups for both genotypes ($p < .05$, diet effect, two-way ANOVA), without genotype effect or interaction (Fig. 4 G-H).

3.8. Amyloid β and nutrient restriction modulate NFκB nuclear translocation on astrocytes in vitro

Astrocytes from the C6 cell line were incubated for 6 h with RPMI supplemented with 10% fetal bovine serum (FBS; non-restricted control condition) or RPMI with 2% FBS (nutrient restricted; NR) and subsequently exposed to fibrillar Aβ 1–42 peptides or vehicle for 2 h. To determine cell activation in response to Aβ peptides and NR we

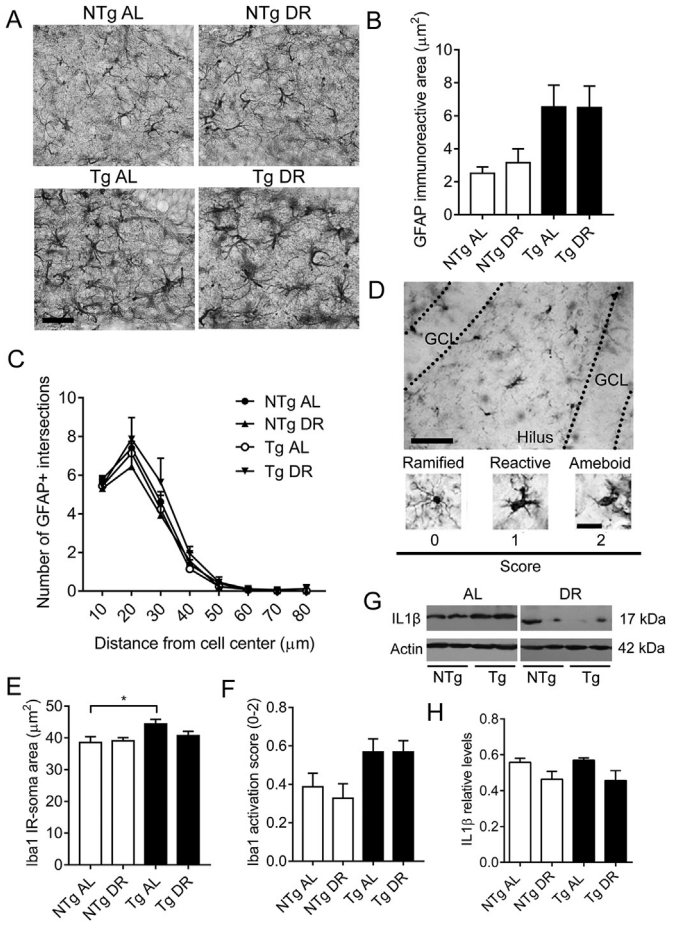

Fig. 4. A. Representative microphotographs of GFAP-stained hippocampal sections. Scale bar: 100 μm. B. GFAP+ immunoreactive area in the hilus of the hippocampus ($p < .01$, genotype effect, two-way ANOVA),. C. Histogram for circle intersections on the Sholl analysis of GFAP+ astrocytes. D. Representative microphotograph of an Iba1 immunostained hippocampal coronal section comprising the granular cell layer (GCL) and the hilus (upper panel) and microphotographs of microglia assigned to each activation state (lower panel). Scale bars: 100 μm (upper panel) and 10 μm (lower panel). E. Iba1+ microglial soma area. *$p < .05$ (Tukey's *post hoc* test, two-way ANOVA). F. Microglia activation score ($p < .05$, genotype effect, two-way ANOVA). $n = 4–6$ animals per group for histological analyses. G. IL1β and actin immunoblotting on hippocampus homogenates. H. IL1β /actin relative levels ($p < .05$, diet effect, two-way ANOVA), $n = 5$ hippocampi per group.

quantified the ratio of nuclear translocation of NFκB on confocal images (Fig. 5 A-B). The quantification showed an effect of amyloid treatment ($p < .05$, two-way ANOVA) and increased translocation in astrocytes exposed to Aβ without NR compared with control (CTL) cells ($p < .05$, Dunnett's *post hoc* test; Fig. 5 A). Both NR CTL and NR Aβ groups were not different from control cells (Dunnett's *post hoc* test). Lipopolysaccharide (LPS) treatment was used as a positive control for NFκB nuclear translocation and compared independently with the CTL group (Student's *t*-test; $p < .05$ LPS *vs.* CTL).

3.9. Direct Aβ exposure or nutrient restriction do not induce changes in NFκB nuclear translocation in microglia in vitro

We exposed BV2 microglia to the same Aβ and NR protocol that was used in astrocytes to evaluate NFκB nuclear translocation (Fig. 5 C-D). Unlike astrocytes, microglia did not show changes in NFκB translocation upon Aβ or NR exposure (Dunnett's *post hoc* test after Two-way ANOVA; Fig. 5 C). Exposure to LPS was used as a positive control for microglial activation and compared independently with the CTL group

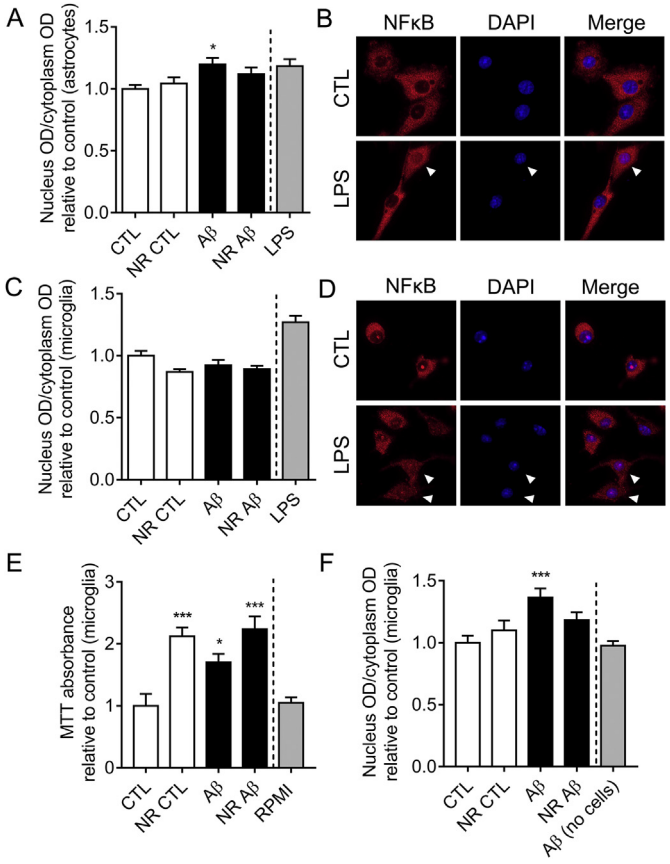

Fig. 5. A and C. NFκB nuclear translocation for Aβ-treated astrocytes (A) and microglia (C). *p < .05 *vs.* CTL (Dunnett's *post hoc* test, two-way ANOVA). Lipopolysaccharide (LPS) was used as a positive control for NFκB nuclear translocation and compared independently with the CTL group (Student's t-test; LPS *vs.* CTL, p < .05 for C6 cells and *p* < .0001 for BV2 cells, significance not shown in the graphs). B and D. Confocal images of NFκB-stained astrocytes (B) and microglia (D) under control conditions (upper panels) or activated after LPS treatment (lower panels). Arrowheads indicate cells with NFκB nuclear translocation. E. Microglial viability evaluated using the MTT assay after exposure to astrocyte-derived conditioned medium. *p < .05 and ***p < .001 *vs.* CTL (Tukey's *post hoc* test, two-way ANOVA). F. NFκB nuclear translocation in conditioned medium-treated microglia. ***p < .001 *vs.* CTL (Dunnett's *post hoc* test, two-way ANOVA), results from at least 25 cells in triplicate samples per group from two independent experiments.

(Student's *t*-test; p < .0001 LPS *vs.* CTL).

3.10. Conditioned media from Aβ- and NR-exposed astrocytes increase microglial viability evidenced by the MTT assay

C6 astrocytes were incubated for 6 h with RPMI +10% FBS (non-restricted control condition) or RPMI +2% FBS (NR) and then transferred to nitrocellulose-coated coverlips with pre-adsorbed Aβ (or vehicle) in RPMI +10% for 2 h. Then, conditioned media (CM) were collected and applied using a 1:1 dilution in RPMI +10% FBS on BV2 microglial cells. The analysis of MTT to formazan conversion showed increased cell viability of BV2 microglia in response to CM from Aβ-treated as well as from NR astrocytes when compared with CM from control cells (Tukey's *pot hoc* test after two-way ANOVA; Fig. 5 E). Conditioned medium from untreated astrocytes was associated with absorbance values similar to those of non-conditioned RPMI-cultured microglia.

3.11. Conditioned medium from Aβ-exposed astrocytes induces NFκB translocation on microglia but not if NR preceded Aβ-exposure

After confirming unspecific increased viability of microglia upon exposure to CM from Aβ- or NR astrocytes, we studied if CM from astrocytes were able to elicit differential activation of microglia, evaluated by NFκB nuclear translocation. We incubated microglia for 2 h with CM from the different astrocyte culture conditions and found interaction between Aβ and nutrient factors ($p < .05$, two-way ANOVA) and an increase of nuclear translocation when comparing the effect of Aβ CM with CTL CM ($p < .001$, Dunnet's *post hoc* test; Fig. 5 F). In order to check for a possible CM-associated effect not mediated by astrocytes and derived from Aβ detaching from nitrocellulose we incubated microglia with medium from cell-free Aβ-coated wells and found that NFκB nuclear translocation level was not different from CTL CM-induced values (Student's *t*-test).

3.12. Autophagy in hippocampal astrocytes and intracellular amyloid in vivo

As mentioned, one of the potentially involved pathways in amyloid processing is autophagy. A double immunofluorescence for LC3 to stain autophagic vesicles and GFAP to identify astrocytes was done on hippocampal sections (Fig. 6 A). A large proportion of the LC3+ areas co-localized with GFAP+ cells while a small percentage corresponded to hilar neurons or vascular regions. Quantification of the proportion of GFAP+ areas also positive for LC3 showed higher levels in transgenic mice, independently of the type of diet (two way ANOVA, $p < .01$ for genotype effect; Fig. 6 B). After confirming that autophagy was occurring in hippocampal astrocytes, we evaluated the relationship of LC3+ autophagic vesicles with amyloid β in the hippocampus of Tg mice. Using a double immunofluorescence for 4G8 to detect Aβ and LC3 for autophagic vesicles (Fig. 6 C) we identified Aβ co-localizing with LC3+ areas in cells that displayed an astrocyte-like morphology (around 5% for both diet groups).

3.13. Nutrient restriction restores autophagic flux in Aβ-treated astrocytes in vitro

In order to study the autophagic flux and amyloid β content in astrocytes using an *in vitro* approach, we exposed astrocytes (C6 cell line) to NR (2% FBS) or control medium (10% FBS) for 6 h, and then to fibrillar Aβ 1–42 peptides for 2, 6 or 24 h to understand the progression of the process. In the last 2 h of incubation, some cell groups were treated with bafilomycin A1 (BAF), a blocker of the autophagic flux, that, when applied to cells in which autophagy is active, causes an accumulation of LC3 due to reduced turnover. Afterward, immunofluorescence techniques to detect LC3 (Autophagosomal marker) and amyloid beta (4G8 antibody) were performed (Fig. 6 D-E). At the 2-h Aβ incubation time, LC3 intracellular levels were not changed by Aβ exposure but were increased after the co-incubation with BAF ($p < .001$ *vs.* every other group, Tukey's *post hoc* test after two-way ANOVA for all the analyses in this subsection, Fig. 6 F), suggesting that autophagy was functional at this time-point. Interestingly, BAF also increased the Aβ content in Aβ-treated cells compared with BAF-naïve cells ($p < .05$, Fig. 6 G), suggesting that autophagy was active and could be involved in amyloid clearance. Also an increased proportion of intracellular Aβ was associated with LC3+ vesicles after BAF treatment, as evidenced by the evaluation of the M2 index for the co-localization of 4G8 and LC3 markers ($p < .01$ *vs.* Aβ and p < .05 *vs.* NR Aβ, Fig. 6 H).

Astrocytes exposed to Aβ peptides for 6 h showed an increase in LC3+ areas (p < .001 *vs.* CTL), an effect that was not seen if the exposure to Aβ was preceded by NR (Fig. 6 I). As co-incubation with BAF attenuated the effect of NR (p < .05 *vs.* NR Aβ), it is reasonable to suggest that the increased levels of LC3 seen in the Aβ group could be

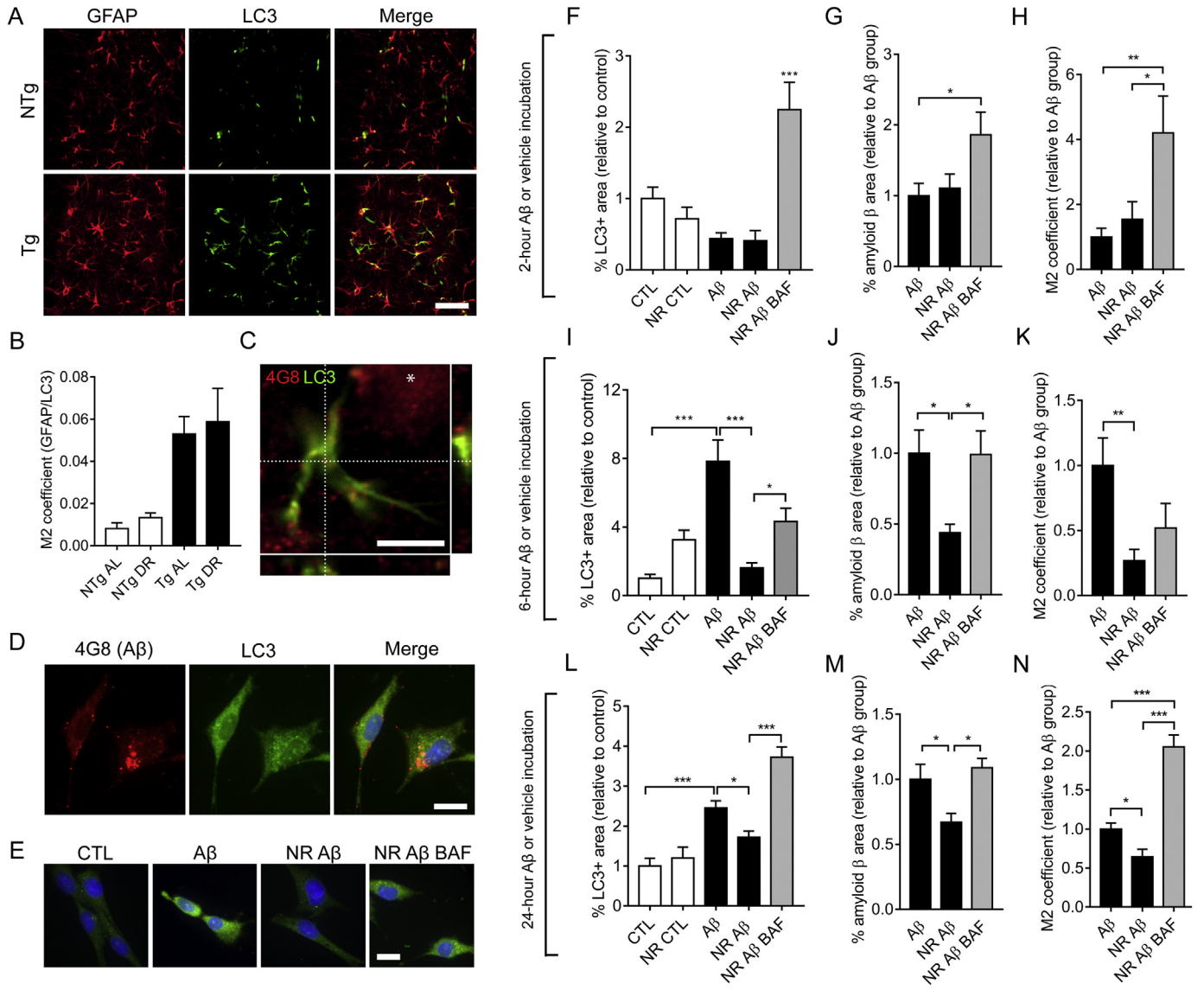

Fig. 6. A. Confocal images of GFAP (red) and LC3 (green) stained hippocampal sections for NTg and Tg experimental groups. Scale bar: 50 μm. B. M2 coefficient (proportion of GFAP+ areas that co-localize with LC3), $n = 4$ animals per group. C. Confocal image of 4G8 (red) and LC3 (green) immunofluorescence in the hilus of the hippocampus of a transgenic mouse showing an amyloid plaque (*) and an LC3+ cell that presents astrocyte morphology with 4G8+ amyloid inside (confirmed in the orthogonal XZ-YZ views). Scale bar: 10 μm. D. Confocal image of Aβ (red) and LC3 (green) immunofluorescence on C6 astrocytes (DAPI in the blue channel). Scale bar: 10 μm. E. Confocal images showing LC3 immunoreactivity in astrocytes from each experimental group with higher intensity in the Aβ and NR Aβ BAF groups. Scale bar: 10 μm. F–N. Quantification of LC3+ and Aβ + percent coverage of C6 cells and M2 coefficient (percentage of Aβ + areas that co-localize with LC3+ areas) for the three Aβ incubation times: F–H corresponding to the 2-h incubation, I–K corresponding to the 6-h incubation and L-N corresponding to the 24-h incubation. *** in E represents $p < .001$ *vs.* every other group. In the other graphs: *$p < .05$, **$p < .01$ and ***$p < .001$ for the indicated comparisons (Tukey's *post hoc* test, two-way ANOVA), results from at least 40 cells per group in triplicate samples from two independent experiments. Mean ± SEM values: % LC3 2 hs CTL 1 ± 0.15, NR CTL 0.71 ± 0.16, Aβ 0.43 ± 0.08, NR Aβ 0.4 ± 0.14, NR Aβ BAF 2.24 ± 0.38; 6 hs CTL 1 ± 0.22, NR CTL 3.24 ± 0.56, Aβ 7.82 ± 1.24, NR Aβ 1.6 ± 0.29, NR Aβ BAF 4.31 ± 0.77; 24 hs CTL 1 ± 0.19, NR CTL 1.19 ± 0.27, Aβ 2.45 ± 0.24, NR Aβ 1.19 ± 0.19, NR Aβ BAF 3.72 ± 0.25. % Aβ: 2 hs Aβ 1 ± 0.177, NR Aβ 1.1 ± 0.2, NR Aβ BAF 1.86 ± 0.32; 6hs Aβ 1 ± 0.16, NR Aβ 0.43 ± 0.05, NR Aβ BAF 0.99 ± 0.16, 24 hs Aβ 1 ± 0.16, NR Aβ 0.49 ± 0.08, NR Aβ BAF 1.08 ± 0.07; M2 index: 2 hs Aβ 1 ± 0.27, NR Aβ 1.54 ± 0.54, NR Aβ BAF 4.2 ± 1.13, 6 hs Aβ 1 ± 0.21, NR Aβ 0.26 ± 0,08, NR Aβ BAF 0.51 ± 0.18, 24 hs Aβ 1 ± 0.1, NR Aβ 0,68 ± 0,1, NR Aβ BAF 2.05 ± 0.15. (For interpretation of the references to colour in this figure legend, the reader is referred to the web version of this article.)

due to blocked autophagy and that NR could be restoring the flux, hence lowering LC3 levels as shown. After a 6-h Aβ incubation, cells that were previously nutrient-restricted had lower levels of Aβ compared with the Aβ-exposed non-restricted group ($p < .05$, Fig. 6 J). This effect was lost after BAF treatment, suggesting that levels of intracellular Aβ deposits depend on a functional autophagic process. Regarding Aβ-LC3 co-localization, a lower percentage of Aβ was found associated to autophagosomes (M2 index; $p < .01$, Fig. 6 K) which in a context of lower levels of intracellular Aβ could indicate degradation or externalization of the amyloid peptide.

Exposure of astrocytes to Aβ for 24 h showed that Aβ-treated cells had higher levels of LC3 compared with controls and that previous NR was able to decrease them to control levels ($p < .001$ for both comparisons, Fig. 6 L), in a similar fashion to what was found in 6-h Aβ-treated cells. Intracellular Aβ and co-localization of Aβ with LC3 were both down-regulated by NR at this time-point ($p < .01$ and $p < .05$, Fig. 6 M and N respectively). Bafilomycin treatment for the last 2 hs of Aβ exposure increased LC3, Aβ and M2 levels ($p < .001$, $p < .05$ and

$p < .001$ respectively for the NR Aβ BAF *vs.* NR Aβ comparison) suggesting that autophagy is functional and involved in the regulation of intracellular amyloid levels.

4. Discussion

Our results provide evidence that a periodic dietary restriction (DR) protocol on an animal model of AD can ameliorate multiple aspects of the pathology. Dietary restriction has been implicated in the reduction of brain amyloid deposits in multiple animal models of AD (Mouton et al., 2009; Patel et al., 2005; Schafer et al., 2015) but underlying mechanisms are not clear yet and many hypotheses have been formulated, mainly pointing either to a decrease in Aβ production or an increase in Aβ clearance. Among the first group, diminished expression of amyloidogenic secretases was described in response to 30% caloric restriction (Schafer et al., 2015) and modulation of APP processing towards the non-amyloidogenic pathway was associated to long-term 30% carbohydrate caloric restriction (Wang et al., 2005), both in the Tg2576 mouse AD model. Among the second group, some authors have suggested that the diet-induced modulation of glial activation could be playing a role in the phagocytosis of Aβ deposits (Patel et al., 2005). Also, as caloric restriction has been associated to the optimization of insulin signaling both peripherally and centrally, increased Aβ clearance could be mediated by decreased competition with insulin for the insulin-degrading enzyme (IDE) degrading activity (Farris et al., 2003).

Autophagy, an important catabolic pathway necessary for the degradation of damaged organelles and aggregated proteins like Aβ could also be involved in the effects of DR. Caloric restriction is a powerful non-pharmacological inducer of the autophagic process (Dong et al., 2015; Yang et al., 2014).and although induction of autophagy as a neuroprotective strategy in AD has been studied mainly in neurons (Lin et al., 2013; Spilman et al., 2010), astroglial autophagy could participate in the uptake or degradation of amyloid peptides (Pomilio et al., 2016; Simonovitch et al., 2016). Also, microglia has been shown to be able to degrade extracellular amyloid fibrils *in vitro* through autophagy (Cho et al., 2014). Our present data shows that a fraction of Aβ co-localizes with LC3+ autophagic vesicles *in vivo* and also *in vitro* and that a substantial proportion of hippocampal LC3+ areas co-localize with the astrocyte marker GFAP, suggesting that astroglial autophagy could be playing a role in amyloid clearance. The analysis of LC3 in hippocampal sections showed increased levels of this protein in GFAP+ astrocytes of Tg mice. However, as autophagy is a dynamic process, this change could be due to an induction of autophagy or could be the result of impaired degradation of autophagosomes, as suggest our *in vitro* results. Also, the lack of effect of DR on astroglial LC3 levels does not necessarily imply an absence of effect on autophagy, as autophagosome formation and degradation could be balanced with no overall changes on LC3 immmunostaining. Further studies should be done in order to clarify these points. At short incubation times with Aβ, *in vitro* astroglial autophagy was not induced, though a certain amount of basal activity was present since bafilomycin treatment increased the LC3-immunoreactive area. Amyloid intracellular levels were higher after bafilomycin exposure indicating that a functional autophagy is necessary to regulate intracellular amyloid content. At longer incubation times (6 and 24 h), Aβ exposure induced higher levels of LC3 astroglial content. Nutrient restriction diminished LC3+ areas to control levels and Aβ cell load to a ~50%. Interestingly, bafilomycin treatment reversed both effects suggesting that NR could be acting through a normalization of the autophagic flux. Unpublished results from our group suggest that Aβ could interrupt the glial autophagic flux through an inhibition of the fusion between the autophagosome and the lysosome, preventing cargo degradation. Also, lysosomal proteolysis malfunction could be a potential subjacent mechanism (Yang et al., 2011). The analysis of the LC3-Aβ co-localization *in vitro* showed that NR decreased the intracellular proportion of Aβ that was contained in autophagic vesicles in a context of lower Aβ levels, suggesting an increase in the degradation or externalization of amyloid peptides as proposed previously (Pomilio et al., 2016). Interestingly, there is evidence that glial autophagy could be induced by inflammatory stimuli and play a role in cell survival under acute inflammation but when blockage of the autophagic flux is also involved, high and non-physiological amounts of ROS are produced by glial cells (Motori et al., 2013), potentially amplifying tissue damage and inflammation propagation. In the present study we describe concomitant glial activation and LC3 accumulation, constituting a highly pro-inflammatory scenario that deserves further research to understand interplaying mechanisms and successful therapeutic interventions.

Reversion of cognitive deficits in the PDAPP-J20 transgenic mice could be mediated by multiple mechanisms. One of the probably involved processes in the cognitive improvement associated to DR is the positive regulation of adult hippocampal neurogenesis. This process is regulated by hormones (Cameron and Gould, 1994), environment (Kempermann et al., 1998), running (van Praag et al., 1999), antidepressants (Malberg et al., 2000), among many other factors, and is likely involved in hippocampal-dependent learning (Marin-Burgin and Schinder, 2012). There is evidence that diet also plays a regulatory role on adult neurogenesis, either inhibiting or stimulating the process. Consumption of high-fat diets has been associated to decreased neurogenesis and synaptic plasticity (Boitard et al., 2012; Lindqvist et al., 2006; Vinuesa et al., 2018; Vinuesa et al., 2016), possibly comprising inflammation and insulin resistance as subjacent elements. On the contrary, dietary restriction positively modulates hippocampal neurogenesis in animal models (Hornsby et al., 2016; Lee et al., 2002) with a potential impact on learning and memory. Among the identified pathways by which DR influences neurogenesis are protection against oxidative stress (Bruce-Keller et al., 1999), neurogenesis-related gene regulation (Wu et al., 2008) and upregulation of neurotrophic factors (Lee et al., 2000; Lee et al., 2002). Other probably underlying pathway was described by Ma et al. as they showed that caloric restriction can improve cognitive performance in control mice through activation of the PI3K/Akt pathways (Ma et al., 2014). Interestingly, one of the signals that can promote cognition in an AD model is hunger, independently of caloric intake (Dhurandhar et al., 2013), pointing to a neuroendocrine regulation of DR effects.

Inflammation and glial activation are present since early stages in models of AD (Beauquis et al., 2014; Li et al., 2011; Pomilio et al., 2016) and mediators such as nitric oxide, TNF, and IL-1β derived from glial cells probably have a role on the pathologic progression. Dietary restriction can have a role in slowing brain aging associated to an attenuation of glial pro-inflammatory activation (Morgan et al., 2007; Sridharan et al., 2013). Caloric restriction is able to decrease astrocyte activation and excitotoxic damage in different murine models of AD (Patel et al., 2005; Zhu et al., 1999). Radler et al. demonstrated that a 50% caloric restriction protocol attenuates LPS-induced microglial activation in discrete regions of mice brains, also suppressing LPS-associated fever (Radler et al., 2014) and pointing towards a general regulation of anti- and pro-inflammatory signals. In the present study we have found a negative regulation of IL1β in the hippocampus of both NTg and Tg mice in response to dietary restriction, suggesting an anti-inflammatory effect. However hippocampal IL1β levels were similar for NTg and Tg animals, indicating that the inflammatory scenario in the PDAPP-J20 Tg mouse at this age is not evidenced by changes in this marker, an observation that is consistent with reports in other models of AD in which inflammatory cytokines are found elevated at later ages (reviewed in Morgan et al., 2005). As our results show, astrocytes are capable of responding *in vitro* both to amyloid peptides and to nutrient restriction and also of transmitting pro- or anti-activation signals to microglia. Activation of microglia after NFκB translocation in astrocytes during neurodegeneration is dependent on several proinflammatory mediators like cytokines IL1β, IL6 and TNFα, ROS (Shih et al., 2015), chemokines (Brambilla et al., 2009) and members of the Wnt family (Ouali Alami et al., 2018), among others. Interestingly, while microglial

cells were activated in an indirect fashion as a response to conditioned media from astrocytes, they did not show activation when directly exposed to these stimuli. This differential response could be due to a number of factors. Sondag et al. showed that primary microglia activation depends on the conformational state of amyloid peptides, finding different degree and quality of activation if using oligomers or fibrils (Sondag et al., 2009). Moreover, though they show similar functional responses, it is possible that BV-2 cells do not respond to Aβ in the same way as primary microglia (Jana et al., 2008). We also hypothesize that astrocytes could be responsive to lower levels of amyloid peptides than microglia and thus able to trigger a functional response to subtle microenvironmental changes. In a mouse model of experimental autoimmune encephalitis, Brambilla et al. have shown that the inactivation of astroglial NFκB reduced CNS inflammation and improved functional recovery, highlighting the regulatory role that astroglia plays in the inflammatory response (Brambilla et al., 2009). Our *in vivo* study showed that dietary restriction prevented the increase in microglia soma size but did not affect astrocytic GFAP immunoreactive area. As these are morphological parameters of glial reactivity that do not provide specific information regarding the functional state of glial cells, a thorough characterization of astroglial and microglial activation using markers for different activation phenotypes is needed to draw solid conclusions.

Activation of glial cells not only correlates with an increase of pro-inflammatory signals but also dampens basic supportive functions affecting the metabolic and energy homeostasis of the nervous system. In this sense, some authors consider AD as a brain metabolic pathology because of the multiple common pathways affected both in AD and metabolic diseases like type 2 diabetes mellitus, obesity, and metabolic syndrome (de la Monte and Tong, 2014) and also because of the data showing brain insulin resistance (Biessels and Reagan, 2015), mitochondrial dysfunction (Demetrius et al., 2014) and disturbed bioenergetics (Sonntag et al., 2017) in patients and experimental models. As astrocytes play a crucial role in brain energy metabolism and neuroprotection, it is plausible to think that loss of these homeostatic functions, as a consequence of pro-inflammatory activation, could be an early and central event in the course of AD, preceding symptomatic phases of the disease (Rodriguez et al., 2009). Lactate derived from glycogen storages in brain astrocytes is considered an emergency fuel during endurance conditions (Matsui et al., 2017) and its availability is dependent on glial homeostatic capability. Peripherally, we found lower glycemic values in Tg mice compared with controls before the beginning of the DR protocol. Although we did not detect hypoglycemia and levels were in a normal range, it is possible that Tg mice have systemic metabolic imbalances, as described in other AD mouse models (Pedros et al., 2014; Vandal et al., 2015). Several studies point to a peripheral pathogenic role for amyloid peptides that could be mediated through pancreatic amyloid co-deposition (reviewed by Wijesekara et al., 2018). Also, inflammatory mediators can have a role on glucose regulation, both centrally and peripherally. In this sense, intracerebroventricular or intraperitoneal injection of IL-1β to mice induces hypoglycemia that is dependent on the action on the central IL-1β receptor (Del Rey et al., 2016). Hence, it is reasonable to propose that diseases associated with CNS inflammation and glial activation can be accompanied by peripheral metabolic disturbances.

Although many epidemiological studies have reported a higher incidence and prevalence of Alzheimer's disease in women, most preclinical research done in mouse models studied male subjects or male and female mice indiscriminately. Taking into account this bias, the present study was performed on female mice to evaluate, as a secondary objective, whether female PDAPP-J20 transgenic animals showed similar pathological progression as male mice. Our results showed that plaque load, neurogenic status and morphological parameters of glial activation paralleled those obtained in previous studies done in male animals (Beauquis et al., 2013; Pomilio et al., 2016). However, subsequent experimental designs including both genders would be desirable to allow the comparison of differential responses.

5. Conclusion

Our results provide evidence of the attenuating effect of dietary restriction on multiple aspects of the pathology in PDAPP-J20 mice, model of Alzheimer's disease. Complementarily, *in vitro* experiments showed that the autophagic process and cell activation are modulated by nutrient restriction in astrocytes exposed to amyloid peptides, suggesting a potential mechanism of action for this strategy. We consider that the lack of overall caloric restriction and weight loss in response to the dietary restriction protocol is an important aspect to be taken into account when dealing with aging-associated conditions (Lee and Longo, 2016). Available data from the basic sciences suggest that dietary restriction could be useful not only for preventing or reducing the risk of AD but also for the reversion of pre-existing brain changes and cognitive deficits. Moreover, there is a great interest in developing dietary restriction-mimetics that eliminate the need for diet changes (Van Cauwenberghe et al., 2016) though we consider that the multiple benefits associated to these dietary habits should not be understated (Mattson and Wan, 2005). Given the lack of effective pharmacological treatments for AD, lifestyle interventions, as multi-target strategies, are potentially valuable alternatives for the prevention and eventual management of the pathology. In this sense, dietary restriction would not only serve as a potential therapeutic strategy *per se*, but also contribute to the in-depth understanding of the pathways involved in the progression of both physiological and pathological aging.

Declarations of Competing Interest

None.

Acknowledgements

This work was supported by Williams, René Barón and Alberto J. Roemmers Foundations, ANPCyT PICT Grants 2013-2645, 2014-1168, 2016-1046 and 2016-1572, CONICET PIP Grant 2013-2015. AG, MFT and JP are recipients of ANPCyT Fellowships. AV, CP, SR and MB are recipients of CONICET Fellowships. SW, FS and JB are CONICET Researchers. The funding sources had no involvement in the study design or the collection, analysis and interpretation of data. We thank Dr. Mónica Kotler's Lab and Dr. Alfredo Lorenzo for technical advice and reagents and Johnson & Johnson Medical S.A. for glycometer reactive strips.

References

Abramoff, M.D., et al., 2004. Image processing with ImageJ. Biophoton. Int. 11, 36–42. https://imagescience.org/meijering/publications/download/bio2004.pdf.

Alirezaei, M., et al., 2011. Autophagy, inflammation and neurodegenerative disease. Eur. J. Neurosci. 33, 197–204. https://doi.org/10.1111/j.1460-9568.2010.07500.x.

Beauquis, J., et al., 2010. Short-term environmental enrichment enhances adult neurogenesis, vascular network and dendritic complexity in the hippocampus of type 1 diabetic mice. PLoS One 5, e13993. https://doi.org/10.1371/journal.pone.0013993.

Beauquis, J., et al., 2013. Environmental enrichment prevents astroglial pathological changes in the hippocampus of APP transgenic mice, model of Alzheimer's disease. Exp.Neurol. 239, 28–37. https://doi.org/10.1016/j.expneurol.2012.09.009.

Beauquis, J., et al., 2014. Neuronal and glial alterations, increased anxiety, and cognitive impairment before hippocampal amyloid deposition in PDAPP mice, model of Alzheimer's disease. Hippocampus 24, 257–269. https://doi.org/10.1002/hipo.22219.

Benda, P., et al., 1968. Differentiated rat glial cell strain in tissue culture. Science 161, 370–371. https://doi.org/10.1126/science.161.3839.370.

Biessels, G.J., Reagan, L.P., 2015. Hippocampal insulin resistance and cognitive dysfunction. Nat. Rev. Neurosci. 16, 660–671. https://doi.org/10.1038/nrn4019.

Boitard, C., et al., 2012. Juvenile, but not adult exposure to high-fat diet impairs relational memory and hippocampal neurogenesis in mice. Hippocampus 22, 2095–2100. https://doi.org/10.1002/hipo.22032.

Bolte, S., Cordelieres, F.P., 2006. A guided tour into subcellular colocalization analysis in light microscopy. J. Microsc. 224, 213–232. https://doi.org/10.1111/j.1365-2818.2006.01706.x.

Bradford, M.M., 1976. A rapid and sensitive method for the quantitation of microgram quantities of protein utilizing the principle of protein-dye binding. Anal. Biochem. 72, 248–254. https://doi.org/10.1006/abio.1976.9999.
Brambilla, R., et al., 2009. Transgenic inhibition of astroglial NF-kappa B improves functional outcome in experimental autoimmune encephalomyelitis by suppressing chronic central nervous system inflammation. J. Immunol. 182, 2628–2640. https://doi.org/10.4049/jimmunol.0802954.
Brandhorst, S., et al., 2015. A periodic diet that mimics fasting promotes multi-system regeneration, enhanced cognitive performance, and healthspan. Cell Metab. 22, 86–99. https://doi.org/10.1016/j.cmet.2015.05.012.
Bruce-Keller, A.J., et al., 1999. Food restriction reduces brain damage and improves behavioral outcome following excitotoxic and metabolic insults. Ann. Neurol. 45, 8–15. https://doi.org/10.1002/1531-8249(199901)45:1<8::AID-ART4>3.0.CO;2-V.
Cameron, A., Gould, E., 1994. Adult neurogenesis is regulated by adrenal steroids in the dentate gyrus. Neuroscience 61, 203–209. https://doi.org/10.1016/0306-4522(94)90224-0.
Cho, M.H., et al., 2014. Autophagy in microglia degrades extracellular beta-amyloid fibrils and regulates the NLRP3 inflammasome. Autophagy 10, 1761–1775. https://doi.org/10.4161/auto.29647.
Combs, C.K., et al., 2001. beta-Amyloid stimulation of microglia and monocytes results in TNFalpha-dependent expression of inducible nitric oxide synthase and neuronal apoptosis. J. Neurosci. 21, 1179–1188. https://doi.org/10.1523/JNEUROSCI.21-04-01179.2001.
de la Monte, S.M., Tong, M., 2014. Brain metabolic dysfunction at the core of Alzheimer's disease. Biochem. Pharmacol. 88, 548–559. https://doi.org/10.1016/j.bcp.2013.12.012.
Del Rey, A., et al., 2016. Brain-borne IL-1 adjusts glucoregulation and provides fuel support to astrocytes and neurons in an autocrine/paracrine manner. Mol. Psychiatry 21, 1309–1320. https://doi.org/10.1038/mp.2015.174.
Demetrius, L.A., et al., 2014. Alzheimer's disease: the amyloid hypothesis and the inverse Warburg effect. Front. Physiol. 5, 522. https://doi.org/10.3389/fphys.2014.00522.
Dhurandhar, E.J., et al., 2013. Hunger in the absence of caloric restriction improves cognition and attenuates Alzheimer's disease pathology in a mouse model. PLoS One 8, e60437. https://doi.org/10.1371/journal.pone.0060437.
Dong, W., et al., 2015. Autophagy involving age-related cognitive behavior and hippocampus injury is modulated by different caloric intake in mice. Int. J. Clin. Exp. Med. 8, 11843–11853. https://www.ncbi.nlm.nih.gov/pmc/articles/PMC4565409/.
Farris, W., et al., 2003. Insulin-degrading enzyme regulates the levels of insulin, amyloid beta-protein, and the beta-amyloid precursor protein intracellular domain in vivo. Proc. Natl. Acad. Sci. U. S. A. 100, 4162–4167. https://doi.org/10.1073/pnas.0230450100.
Ferreira, T.A., et al., 2014. Neuronal morphometry directly from bitmap images. Nat. Methods 11, 982–984. https://doi.org/10.1038/nmeth.3125.
Halagappa, V.K., et al., 2007. Intermittent fasting and caloric restriction ameliorate age-related behavioral deficits in the triple-transgenic mouse model of Alzheimer's disease. Neurobiol. Dis. 26, 212–220. https://doi.org/10.1016/j.nbd.2006.12.019.
Hornsby, A.K., et al., 2016. Short-term calorie restriction enhances adult hippocampal neurogenesis and remote fear memory in a Ghsr-dependent manner. Psychoneuroendocrinology 63, 198–207. https://doi.org/10.1016/j.psyneuen.2015.09.023.
Jana, M., et al., 2008. Fibrillar amyloid-beta peptides activate microglia via TLR2: implications for Alzheimer's disease. J. Immunol. 181, 7254–7262. https://doi.org/10.4049/jimmunol.181.10.7254.
Kempermann, G., et al., 1998. Experience-induced neurogenesis in the senescent dentate gyrus. J. Neurosci. 18, 3206–3212. https://doi.org/10.1523/JNEUROSCI.18-09-03206.1998.
Lagenaur, C., Lemmon, V., 1987. An L1-like molecule, the 8D9 antigen, is a potent substrate for neurite extension. Proc. Natl. Acad. Sci. U. S. A. 84, 7753–7757. https://doi.org/10.1073/pnas.84.21.7753.
Lee, C., Longo, V., 2016. Dietary restriction with and without caloric restriction for healthy aging. F1000Res 5. https://doi.org/10.12688/f1000research.7136.1.
Lee, J., et al., 2000. Dietary restriction increases the number of newly generated neural cells, and induces BDNF expression, in the dentate gyrus of rats. J. Mol. Neurosci. 15, 99–108. https://doi.org/10.1385/JMN:15:2:99.
Lee, J., et al., 2002. Evidence that brain-derived neurotrophic factor is required for basal neurogenesis and mediates, in part, the enhancement of neurogenesis by dietary restriction in the hippocampus of adult mice. J.Neurochem. 82, 1367–1375. https://doi.org/10.1046/j.1471-4159.2002.01085.x.
Li, C., et al., 2011. Astrocytes: implications for neuroinflammatory pathogenesis of Alzheimer's disease. Curr. Alzheimer Res. 8, 67–80. https://doi.org/10.2174/156720511794604543.
Lin, A.L., et al., 2013. Chronic rapamycin restores brain vascular integrity and function through NO synthase activation and improves memory in symptomatic mice modeling Alzheimer's disease. J. Cereb. Blood Flow Metab. 33, 1412–1421. https://doi.org/10.1038/jcbfm.2013.82.
Lindqvist, A., et al., 2006. High-fat diet impairs hippocampal neurogenesis in male rats. Eur. J. Neurol. 13, 1385–1388. https://doi.org/10.1111/j.1468-1331.2006.01500.x.
Liu, Y., et al., 2017. Short-term caloric restriction exerts neuroprotective effects following mild traumatic brain injury by promoting autophagy and inhibiting astrocyte activation. Behav. Brain Res. 331, 135–142. https://doi.org/10.1016/j.bbr.2017.04.024.
Luchsinger, J.A., et al., 2002. Caloric intake and the risk of Alzheimer disease. Arch. Neurol. 59, 1258–1263. https://doi.org/10.1001/archneur.59.8.1258.
Ma, L., et al., 2014. Caloric restriction can improve learning ability in C57/BL mice via regulation of the insulin-PI3K/Akt signaling pathway. Neurol. Sci. 35, 1381–1386. https://doi.org/10.1007/s10072-014-1717-5.
Ma, L., et al., 2018. Caloric restriction can improve learning and memory in C57/BL mice probably via regulation of the AMPK signaling pathway. Exp. Gerontol. 102, 28–35. https://doi.org/10.1016/j.exger.2017.11.013.
Malberg, J.E., et al., 2000. Chronic antidepressant treatment increases neurogenesis in adult rat hippocampus. J. Neurosci. 20, 9104–9110. https://doi.org/10.1523/JNEUROSCI.20-24-09104.2000.
Marin-Burgin, A., Schinder, A.F., 2012. Requirement of adult-born neurons for hippocampus-dependent learning. Behav. Brain Res. 227, 391–399. https://doi.org/10.1016/j.bbr.2011.07.001.
Matsui, T., et al., 2017. Astrocytic glycogen-derived lactate fuels the brain during exhaustive exercise to maintain endurance capacity. Proc. Natl. Acad. Sci. U. S. A. 114, 6358–6363. https://doi.org/10.1073/pnas.1702739114.
Mattson, M.P., 2005. Energy intake, meal frequency, and health: a neurobiological perspective. Annu. Rev. Nutr. 25, 237–260. https://doi.org/10.1146/annurev.nutr.25.050304.092526.
Mattson, M.P., Wan, R., 2005. Beneficial effects of intermittent fasting and caloric restriction on the cardiovascular and cerebrovascular systems. J. Nutr. Biochem. 16, 129–137. https://doi.org/10.1016/j.jnutbio.2004.12.007.
McCay, C.M., et al., 1935. The effect of retarded growth upon the length of life span and upon the ultimate body size. J. Nutr. 10, 63–79. https://doi.org/10.1093/jn/10.1.63.
Mladenovic Djordjevic, A., et al., 2010. Long-term dietary restriction modulates the level of presynaptic proteins in the cortex and hippocampus of the aging rat. Neurochem. Int. 56, 250–255. https://doi.org/10.1016/j.neuint.2009.10.008.
Morgan, D., et al., 2005. Dynamic complexity of the microglial activation response in transgenic models of amyloid deposition: implications for Alzheimer therapeutics. J. Neuropathol. Exp. Neurol. 64, 743–753. https://doi.org/10.1097/01.jnen.0000178444.33972.e0.
Morgan, T.E., et al., 2007. Anti-inflammatory mechanisms of dietary restriction in slowing aging processes. Interdiscip. Top. Gerontol. 35, 83–97. https://doi.org/10.1159/000096557.
Moroi-Fetters, S.E., et al., 1989. Dietary restriction suppresses age-related changes in dendritic spines. Neurobiol. Aging 10, 317–322. https://doi.org/10.1016/0197-4580(89)90042-0.
Motori, E., et al., 2013. Inflammation-induced alteration of astrocyte mitochondrial dynamics requires autophagy for mitochondrial network maintenance. Cell Metab. 18, 844–859. https://doi.org/10.1016/j.cmet.2013.11.005.
Mouton, P.R., et al., 2009. Caloric restriction attenuates amyloid deposition in middle-aged dtg APP/PS1 mice. Neurosci. Lett. 464, 184–187. https://doi.org/10.1016/j.neulet.2009.08.038.
Mucke, L., et al., 2000. High-level neuronal expression of abeta 1-42 in wild-type human amyloid protein precursor transgenic mice: synaptotoxicity without plaque formation. J.Neurosci. 20, 4050–4058. https://doi.org/10.1523/JNEUROSCI.20-11-04050.2000.
Ngandu, T., et al., 2015. A 2 year multidomain intervention of diet, exercise, cognitive training, and vascular risk monitoring versus control to prevent cognitive decline in at-risk elderly people (FINGER): a randomised controlled trial. Lancet 385, 2255–2263. https://doi.org/10.1016/S0140-6736(15)60461-5.
Nilsson, P., et al., 2013. Abeta secretion and plaque formation depend on autophagy. Cell Rep. 5, 61–69. https://doi.org/10.1016/j.celrep.2013.08.042.
Olabarria, M., et al., 2010. Concomitant astroglial atrophy and astrogliosis in a triple transgenic animal model of Alzheimer's disease. Glia 58, 831–838. https://doi.org/10.1002/glia.20967.
Ouali Alami, N., et al., 2018. NF-kappaB activation in astrocytes drives a stage-specific beneficial neuroimmunological response in ALS. EMBO J. 37. https://doi.org/10.15252/embj.201798697.
Patel, N.V., et al., 2005. Caloric restriction attenuates Abeta-deposition in Alzheimer transgenic models. Neurobiol. Aging 26, 995–1000. https://doi.org/10.1016/j.neurobiolaging.2004.09.014.
Pedros, I., et al., 2014. Early alterations in energy metabolism in the hippocampus of APPswe/PS1dE9 mouse model of Alzheimer's disease. Biochim. Biophys. Acta 1842, 1556–1566. https://doi.org/10.1016/j.bbadis.2014.05.025.
Pomilio, C., et al., 2016. Glial alterations from early to late stages in a model of Alzheimer's disease: evidence of autophagy involvement in Abeta internalization. Hippocampus 26, 194–210. https://doi.org/10.1002/hipo.22503.
Radler, M.E., et al., 2014. Calorie restriction attenuates lipopolysaccharide (LPS)-induced microglial activation in discrete regions of the hypothalamus and the subfornical organ. Brain Behav. Immun. 38, 13–24. https://doi.org/10.1016/j.bbi.2013.11.014.
Rodriguez, J.J., et al., 2009. Astroglia in dementia and Alzheimer's disease. Cell Death Differ. 16, 378–385. https://doi.org/10.1038/cdd.2008.172.
Schafer, M.J., et al., 2015. Reduction of beta-amyloid and gamma-secretase by calorie restriction in female Tg2576 mice. Neurobiol. Aging 36, 1293–1302. https://doi.org/10.1016/j.neurobiolaging.2014.10.043.
Shih, R.H., et al., 2015. NF-kappaB signaling pathways in neurological inflammation: a mini review. Front. Mol. Neurosci. 8, 77. https://doi.org/10.3389/fnmol.2015.00077.
Simonovitch, S., et al., 2016. Impaired autophagy in APOE4 astrocytes. J. Alzheimers Dis. 51, 915–927. https://doi.org/10.3233/JAD-151101.
Sondag, C.M., et al., 2009. Beta amyloid oligomers and fibrils stimulate differential activation of primary microglia. J. Neuroinflammation 6, 1. https://doi.org/10.1186/1742-2094-6-1.
Sonntag, K.C., et al., 2017. Late-onset Alzheimer's disease is associated with inherent changes in bioenergetics profiles. Sci. Rep. 7, 14038. https://doi.org/10.1038/s41598-017-14420-x.
Spilman, P., et al., 2010. Inhibition of mTOR by rapamycin abolishes cognitive deficits and reduces amyloid-beta levels in a mouse model of Alzheimer's disease. PLoS One 5, e9979. https://doi.org/10.1371/journal.pone.0009979.

Sridharan, A., et al., 2013. Calorie restriction attenuates astrogliosis but not amyloid plaque load in aged rhesus macaques: a preliminary quantitative imaging study. Brain Res. 1508, 1–8. https://doi.org/10.1016/j.brainres.2013.02.046.

Tamura, B.K., et al., 2007. Weight loss in patients with Alzheimer's disease. J. Nutr. Elder. 26, 21–38. https://doi.org/10.1300/J052v26n03_02.

Van Cauwenberghe, C., et al., 2016. Caloric restriction: beneficial effects on brain aging and Alzheimer's disease. Mamm. Genome 27, 300–319. https://doi.org/10.1007/s00335-016-9647-6.

van Praag, H., et al., 1999. Running increases cell proliferation and neurogenesis in the adult mouse dentate gyrus. Nat. Neurosci. 2, 266–270. https://doi.org/10.1038/6368.

Vandal, M., et al., 2015. Age-dependent impairment of glucose tolerance in the 3xTg-AD mouse model of Alzheimer's disease. FASEB J. 29, 4273–4284. https://doi.org/10.1096/fj.14-268482.

Vinuesa, A., et al., 2016. Juvenile exposure to a high fat diet promotes behavioral and limbic alterations in the absence of obesity. Psychoneuroendocrinology. 72, 22–33. https://doi.org/10.1016/j.psyneuen.2016.06.004.

Vinuesa, A., et al., 2018. Early exposure to a high-fat diet impacts on hippocampal plasticity: implication of microglia-derived exosome-like extracellular vesicles. Mol. Neurobiol. https://doi.org/10.1007/s12035-018-1435-8.

Wang, J., et al., 2005. Caloric restriction attenuates beta-amyloid neuropathology in a mouse model of Alzheimer's disease. FASEB J. 19, 659–661. https://doi.org/10.1096/fj.04-3182fje.

Wijesekara, N., et al., 2018. Impaired peripheral glucose homeostasis and Alzheimer's disease. Neuropharmacology 136, 172–181. https://doi.org/10.1016/j.neuropharm.2017.11.027.

Wu, P., et al., 2008. Calorie restriction ameliorates neurodegenerative phenotypes in forebrain-specific presenilin-1 and presenilin-2 double knockout mice. Neurobiol. Aging 29, 1502–1511. https://doi.org/10.1016/j.neurobiolaging.2007.03.028.

Yang, D.S., et al., 2011. Therapeutic effects of remediating autophagy failure in a mouse model of Alzheimer disease by enhancing lysosomal proteolysis. Autophagy 7, 788–789. https://doi.org/10.4161/auto.7.7.15596.

Yang, F., et al., 2014. mTOR and autophagy in normal brain aging and caloric restriction ameliorating age-related cognition deficits. Behav. Brain Res. 264, 82–90. https://doi.org/10.1016/j.bbr.2014.02.005.

Zhu, H., et al., 1999. Dietary restriction protects hippocampal neurons against the death-promoting action of a presenilin-1 mutation. Brain Res. 842, 224–229. https://doi.org/10.1016/S0006-8993(99)01827-2.